Modeling, Design, and Optimization of Mindwalker Series Elastic Joint

Shiqian Wang, Cor Meijneke
Biomechanical Engineering Dept.
Delft University of Technology (TU Delft)
Delft, the Netherlands
shiqian.wang@tudelft.nl

Herman van der Kooij
Biomechatronics and Rehabilitation Technology
University of Twente
Enschede, the Netherlands
Biomechanical Engineering Dept.
Delft University of Technology,
Delft, the Netherlands
h.vanderkooij@utwente.nl

***Abstract*—Weight and power autonomy are limiting the daily use of wearable exoskeleton. Lightweight, efficient and powerful actuation system are not easy to achieve. Choosing the right combinations of existing technologies, such as battery, gear and motor is not a trivial task. In this paper, we propose an optimization framework by setting up a power-based quasi-static model of the exoskeleton joint drivetrain. The goal is to find the most efficient and lightweight combinations. This framework can be generalized for other similar applications by extending or accommodating the model to their own needs. We also present the Mindwalker exoskeleton joint, for which a novel series elastic actuator, consisting of a ballscrew-driven linear actuator and a double spiral spring, was developed and tested. This linear actuator is capable of outputting 960W power and the exoskeleton joint can output 100Nm peak torque continuously. The double spiral spring can sense torque between 0.08Nm and 100Nm and it exhibits linearity of 99.99%, with no backlash or hysteresis. The series elastic joint can track a chirp torque profile with amplitude of 100Nm over 6Hz (large torque bandwidth) and for small torque (2Nm peak-to-peak), it has a bandwidth over 38Hz. The integrated exoskeleton joint, including the ballscrew-driven linear actuator, the series spring, electronics and the metal housing which hosts these components, weighs 2.9kg.**

Keywords—wearable; exoskeleton; series elastic actuation; SEA; spiral spring; power based quasi-static modeling

I. INTRODUCTION

Spinal cord injury (SCI) has high personal impact and socio-economic consequences. Patients with SCI involuntarily place a heavy burden on the health care system. According to the Wyndaele's review in 2006 [1], prevalence of SCI in northern America and Europe was estimated to be 485 per million population, with a range of 223-755 per million population; reported incidence of SCI lies between 10.4 and 83 per million inhabitants per year worldwide. Two thirds of patients are estimated to be paraplegic. Most patients with SCI are young men in the beginning of their thirties, who need to work to support their families, but now have to rely on help from heath care system and social security system.

Exoskeletons are introduced in the rehabilitation market, in attempt to mitigate the aforementioned problems, out of which ReWalk, Ekso, and REX are the most advanced and mature systems. ReWalk [2], Ekso [3] are relatively lightweight (20~25kg) but still rely on the help of crutches to maintain balance and compensate the power insufficiency in the exoskeleton joints. The lack of actuation in some degrees of freedom such as the ankle joint, prevents the daily application of these exoskeletons, simply because without crutches or the help of others, it is almost impossible for a patient to stand up from sitting position. REX [4] exoskeleton is fully actuated but much heavier (38kg); it is inconvenient to be worn daily. All three exoskeletons use electric motors due to their excellent controllability and ease of supplying power, compared with other actuators such as hydraulic and pneumatic actuators. However, in most of the current designs, the relative low power and torque density of the electric motor result in either a heavy or a functionally limited system. Further, these exoskeletons use position-controlled rather than force-controlled actuators; position-controlled actuators are potentially unsafe during contact transitions [5], especially when interacting with human. Mina exoskeleton [9] which uses force controllable actuators is still in an evaluation phase. It also only has hip and knee actuation in sagittal plane, but it weighs already over 21 kg.

Based on above analysis we could conclude that weight is the factor that limits the daily use of a wearable exoskeleton. The weight of actuators, and the weight of batteries. When weight becomes critical, choosing proper components for the joint drivetrain becomes difficult. The often encountered questions are

- Should we sacrifice the weight of the battery for heavier but more efficient motors, or vice versa? In general, larger motors are more efficient than smaller motors[1]; a more

[1] Qualitative explanation: **a**) copper loss $i_M^2 R_M = (T_M / K_T)^2 R_M$ is the main loss in a permanent magnetic brushless DC (PMBLDC) motor, where i_M is current, R_M winding resistance, T_M motor torque, and K_T torque constant. Keeping the required torque, flux density and winding wire cross-section area constant, winding resistance and torque constant is proportional to the number of winding turns. Motor size (weight) can be increased by increasing the winding turns by k, but the copper loss will decrease by a factor of $1/k$; i.e., less heat and higher efficiency **b**) larger motors with increased winding turns, has proportionally more surface through which they can release heat (remember winding resistance increases as temperature rises).

978-1-4673-6024-1/13/$31.00 ©2013 IEEE

efficient motor demands smaller battery, but the motor itself is heavier.

- How to match a gear system with a motor so that the overall efficiency is maximized and the battery size is minimized?

The goal of this paper is to investigate whether a *lightweight* exoskeleton design could be realized by using torque controlled series elastic actuators (SEA). The exoskeleton is supposed to help SCI induced paraplegics to walk again; it is named as Mindwalker since the ultimate goal is to use brain signal to control the exoskeleton [6]. In this paper we try to setup a simple model of the exoskeleton joint drivetrain consisting of the series spring, the gear system, the motor, drive electronics and the battery, based on which a two-step optimization framework is proposed to tackle the aforementioned problems, namely, to find the proper gear ratio (in our case it is the geometrical parameters of the design) so that energy consumption is minimized, and to find the best combination of gear, motor and battery so that their total weight is minimal. Similar approach has been widely applied in modeling hybrid electrical vehicle (HEV) drivetrain and energy management system (see e.g. [7]), where fuel consumption (efficiency) is minimized but not the total weight of the vehicle drivetrain. The proposed approach can be accommodated for similar applications, e.g. by replacing the ballascrew for other type of gear system, or by replacing the simple component model with a more advanced or detailed model.

In this paper, we first specify the design requirements and describe the design concept of the new SEA in section II. In section III, the power-based drivetrain modeling and design optimization framework is explained, followed by discussions. In section IV, the design details of Mindwalker exoskeleton joint is presented. In section V, the preliminary tests results are given. Conclusions are given in section VI.

II. Design Requirements and Concept of the Exoskeleton Joint

A. Design Requirements

In this exoskeleton, four degrees of freedom (DOFs) will be actuated: the hip flexion/extension (HFE), hip abduction/adduction (HAA), knee flexion/extension (KFE), and ankle dorsi/plantar flexion (ADP). We believe with these powered and other passive DOFs, straight level-ground walking could be realized. We are targeting at a user group with maximal body weight 100kg, and a walking speed of 0.8 m/s. We collected and analyzed human gait data to facilitate the design by providing information such as joint velocity, torque and power [8]. A list of design requirements are given in Table I.

TABLE I. Design Requirements for an Exoskeleton Joint

Peak torque	100 Nm
Peak power	>150 W
Series spring stiffness	800 Nm/rad
Small torque bandwidth@2Nm	20 Hz
Large torque bandwidth@100Nm	4 Hz
Output torque resolution	1 Nm
Closed-loop control update frequency	1000Hz
Joint mass	As light as possible

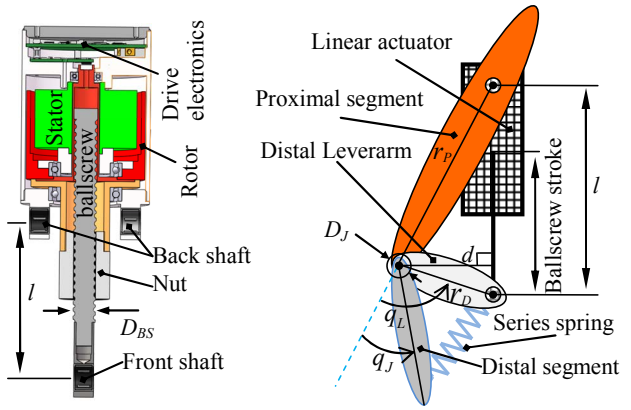

Fig. 1. **Left:** Linear actuator. Both outrunner motors (stator inside of rotor) and inrunner motors (rotor inside of stator) can be implemented, provided the core is hollow. In this concept, the ballscrew nut is directly coupled to the rotor; the screw can retract into the core of the motor; the drive electronics is mounted at the back of the stator. These decisions result in a very compact linear actuator design. **Right**: SEA concept. The series spring decouples the load from the linear actuator. By sensing the spring deflection, joint torque could be measured. r_P = proximal leverarm; r_D = distal leverarm; d = moment arm; q_L = leverarm angle, q_J = joint angle; l = distance between the actuator shafts; D_{BS} = ballscrew diameter; D_J = joint shaft diameter.

B. Actuation Concept

To make the exoskeleton joint force/torque controllable, a series elastic actuator (SEA) will be implemented. The basic concept is depicted in Fig 1. The SEA consists of a custom-made linear actuator and a torsion series spring. The linear actuator integrates a brushless direct current (BLDC) motor, and a ballscrew. In the linear actuator, the ballscrew nut is directly coupled to rotor. The hollow structure allows the ballscrew to pass through the heart of the motor stator, which makes the linear actuator very compact. The housing of linear actuator connects to the proximal segment and the ballscrew pushes and pulls the distal leverarm, which is elastically coupled to the distal segment via the torsion spring. By sensing the spring deflection, the joint torque can be measured directly. The torsion spring design will be elaborated in section III B.

In the modeling and optimization of the joint drivetrain, motors, ballscrews, size of the battery are free to change. Geometrical parameters which contribute to the total gear ratio, i.e., the proximal leverarm r_P, the distal leverarm r_P, and the initial angle q_{L0} between them when standing, are optimized.

C. Component Selections

Ballscrews are chosen as the transmission because of its high torque density, high efficiency, and good backdrivability. Harmonic drives are often used for robots thanks to its relative high torque density and easy integration with rotary motors [9]. However harmonic drive suffers from low efficiency and poor backdrivability; similar story holds for lead screw, if no special development effort is implemented [10]; planetary gear is ruled out due to its low torque density.

By assuming a moment arm d between 40~60mm, the required axial load and peak rotating speed of ballscrews can be estimated from the gait data [8]. In this paper we limit our investigation to three candidate ballscrews SKF SD12x4, SKF SD12x5, and SKF SD10x4. These ballscrews satisfy the torque

(given a safety factor of about 2) and velocity demand, and they can pass through the hollow stators of most candidate motors. In reality we did have compared more ballscrews and motors, which will not be listed due to limited space.

TABLE II. CANDIDATE BALLSCREWS

Type	SKF SD12x5	SKF SD10x4	SKF SD12x4
Theoretical forward efficiency)[a]	0.956	0.954	0.946
Theoretical backdrive efficiency	0.954	0.952	0.943
Dynamic load rating (N)	4200	4500	5000
Static load rating (N)	5300	5400	5000
Nut mass (kg)	0.058	0.040	0.066
Nut inertia (kg·mm^2)	4.89	2.71	6.55
Screw mass (kg/m)	0.71	0.43	0.71

[a] practical forward efficiency is 0.9 times of theoretical efficiency.

For motor selection, efficiency and torque density are the quantities of interest. Permanent magnetic brushless DC motors generally have relatively higher torque density and efficiency. Copper loss is the main loss in this type of motor. Motor constant K_M is a figure of merit used to compare the relative efficiencies and output power capabilities of different motors, which defines the ability of the motor to transform electrical power to mechanical power [11]. Motors from different suppliers, such as Maxon, Moog, Emoteq and model airplane motor suppliers such as Dualsky, E-flite, and Hacker, are selected according to the torque and power requirements for all joints assuming a gear ratio ranging from 50:1 to 126:1 ($2\pi d/p_{BS}$, with p_{BS} the ballscrew lead). Then the motors are sorted using motor constant in ascending order, of which the top ten are shown in Table III.

TABLE III. CANDIDATE MOTORS

#	1	2	3	4	5
Type	Dualsky XM5060 EA10	E-Flite 110BL	Hacker A50-12L V2	Hacker A50-16L V2	Hacker A50-14L V2
Torque const. (Nm/A)	0.033	0.032	0.027	0.035	0.032
Winding resistance(Ω)	0.040	0.030	0.021	0.031	0.025
Motor const.(Nm/$\sqrt{\text{W}}$)	0.165	0.187	0.189	0.199	0.201
Weight (kg)	0.376	0.490	0.430	0.430	0.430
#	**6**	**7**	**8**	**9**	**10**
Type	E-Flite 90BL	Dualsky XM6350 EA15	Dualsky XM6350 EA12	Hacker A60-7S V2	Dualsky XM6360 EA12
Torque const. (Nm/A)	0.029	0.043	0.034	0.044	0.052
Winding resistance(Ω)	0.020	0.041	0.025	0.026	0.034
Motor const.(Nm/$\sqrt{\text{W}}$)	0.208	0.211	0.216	0.276	0.282
Weight (kg)	0.450	0.453	0.462	0.595	0.617

From motor construction point of view, outrunners (stator inside) can achieved relatively higher efficiency and torque density than inrunners (rotor inside), because a) better filling factors (more winding turns, therefore higher torque density) could be achieved in the stator of outrunners, b) higher winding factor (determined by pole and slot numbers) could be obtained [11][12]. This explains why in Table III, no inrunner motor is present. Different from other applications, bipedal walking is a typical low-speed-high-torque application, for which outrunner motors are normally optimized. Furthermore, the cyclic gait pattern requires, in the beginning and end of a stride, the system states (e.g., velocities and accelerations) are recovered, meaning, the acceleration (where inertia costs energy) and deceleration (where inertia helps to brake) phases are more or less evenly distributed. Therefore the relatively higher rotor inertia is not considered as a major disadvantage. We will look at the possible losses due to rotor inertia in section III D.

We did not use helical compression springs as series springs, because the required preload on the antagonistic (or back-to-back) pairs can waste half of the spring energy capacity (redundant mass). Therefore we made a special series spring, of which the design will be elaborated in section III B.

III. JOINT DESIGN OPTIMIZATION

A. Notation Conventions

The analysis and optimization of the joint drivetrain involves large number of quantities, for ease of reference a list of principle symbols is given below. In each component model in the drivetrain, symbols with suffix $_1$ represent the input quantities of that component, e.g., P_{M1} is the input power of the motor; accordingly symbols with suffix $_2$ output quantities; power and energy terms without suffix are the powers and energies dissipated (or added) by that component, e.g., P_{BS} and ΔE_{BS} is the power and energy loss of the ballscrew. Powers flowing from the input port to the output port are defined as positive. Forward efficiencies are suffixed by $_{12}$ and backdrive efficiencies by $_{21}$.

For all time-dependent variables, such as joint torques, joint powers, joint angles, motor torques and velocities, etc., time is dropped out for simplicity. Time derivatives are indicated by dot, e.g., $\dot{q}_J$ is the joint velocity. Quantities in this paper are in *SI base units* if not specified.

TABLE IV. CONSTANTS AND VARIABLES

Symbol	Quantity	Symbol	Quantity	Symbol	Quantity
Constants					
η_{BS12}	Ballscrew forward efficiency	η_{BS21}	Ballscrew backdrive efficiency	k_S	Series spring stiffness
η_{B12}	Battery discharge efficiency	η_{B21}	Battery charge efficiency	J_M	Lumped rotor moment of inertia
η_{4q12}	Motor drive forward efficiency	η_{4q21}	Motor drive braking efficiency	U_S	Motor supply voltage
Time-Dependent Variables					
P_J	Joint output power	P_{BS2}	Ballscrew output power	q_J	Joint angle
P_{S2}	Series spring output power	P_{BS1}	Ballscrew input power	q_L	Leverarm angle
P_{S1}	Series spring input power	P_{Cu}	Copper loss of motor	q_S	Series spring deflection
P_{M2}	Motor output power	P_{4q1}	Drive electronics input power		
P_{M1}	Motor input power	P_{B1}	Battery input power		

B. Series Spring Design and Weight Minimization

Springs made of a single piece of material requires no preload and could be more lightweight. We designed and produced a disk-shaped double spiral spring (Fig. 2), which is a continuation of the idea from Stienen [13] and Lagoda [14]. This new design aims to improve in torque density, and the accuracy of spring stiffness estimation, and to eliminate

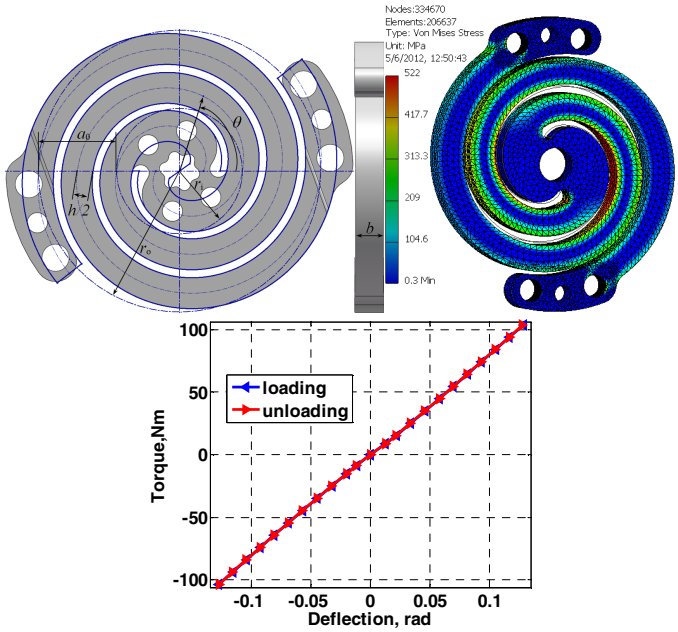

Fig. 2**: Top-left:** double spiral spring: r_i = root diameter; r_o= outer diameter; a_0 = space (pitch) between coils of one spiral; h = spiral thickness; b = spring width; θ = parametric angle ($\theta = 0$ is the root, $\theta = 2\pi$ is one revolution); n (not shown) = active spiral coils (revolutions, denoted as n_0 when no load is applied. In this figure each spiral branch has $n_0 = 1$); **Top-right:** finite element analysis on the stress in the spiral spring when 100Nm torque is applied; it can be seen that the peak stress 522MPa is slightly over the material fatigue strength (510MPa). After applying all the correcting factors we conclude that for repetitive 100Nm peak to peak loading cycle, the spring service life is about 0.14 million cycle. **Bottom:** spring load-deflection curve. The spring exhibits highly linear behavior, and zero backlash at the connection spots. The linearity is estimated to be over 99.99%.

connection backlash.

1) Double spiral spring

The spiral spring consists of two Archimedean spirals. The edges of the spiral spring are two curves equally offset a certain distance (h/2) from the Archimedean spirals (centerline).

2) Spring weight minimization

This double spiral spring was made from a single piece of high grade titanium for its low mass index ($\rho_S Y_S/S_f^2$, ρ_S = mass density; Y_S = Young's modulus; S_f = fatigue strength).

The spring geometry (b, h and a_0) is optimized to reduce mass. Given the design space we have, we fixed the parameters such as r_i = 18.5mm and r_o = 41.5mm (see Fig. 2, top-left). We formulate the objective function as the spring mass

$$\min M_S(b,h,a_0) = \rho_S bh \frac{\pi\left(r_o^2 - r_i^2\right)}{h + a_0} \tag{1}$$

subjected to constraints:

$$\begin{cases} n_0 = (r_o - r_i)/(h + a_0) \geq 1 \text{ active coil number } \geq 1 \\ \sigma_{\max} \leq S_f / C_{s,\sigma} \text{ max. stress below fatigue strength } S_f \\ q_{S\max} \leq q_{Swound} / C_{s,touch} \text{ no touching at max. deflection} \\ k_S = k_{Sdes} \text{ desired stiffness } k_{Sdes} = 800\text{Nm/rad} \end{cases}$$

where $C_{S,\sigma}$ and $C_{S,touch}$ are safety factors; $q_{S\max}$ and q_{Swound} are the spring maximal deflection and the deflection when its spirals are fully wound respectively.

Optimal values were found when b = 10.46mm, h = 9.12mm and a_0 =13.88mm. Each of the spirals has an active coil number n_0 = 1. The mass of the spring is about 220gram.

The stress distribution and stiffness are checked using finite element analysis tool (Inventor 2011); its stiffness is experimentally validated (see Fig. 2). The measured stiffness is 820Nm/rad, with a prediction error less than 2.5%. The spring exhibits highly linear behavior (linearity over 99.99%), and there is no backlash at the connections.

C. Power-Based Quasi-static Model of the SEA Drivetrain

We try to model all the components in the drivetrain including the series spring, the gear system, the motor, the drive electronics and the battery. The modeling procedure starts with collecting gait data

$$\begin{aligned} & q_J && \text{joint angle} \\ & T_J = T_S && \text{joint torque = spring torque} \\ & P_J = \dot{q}_J \cdot T_J = P_{S2} && \text{joint power = spring output power} \end{aligned} \tag{2}$$

1) Series spring

The series spring mass/inertia is lumped to distal segment (load side). The input power to the series spring (equal to the output power of the ballscrew) is

$$P_{S1} = \dot{q}_L \cdot T_S = \left(\dot{q}_J + \dot{T}_J / k_S\right) \cdot T_J = P_{BS2} \tag{3}$$

2) Gear system

The gear system consists of a ballscrew and a leverarm. Assuming piecewise linear losses (forward- and back-driving with different constant efficiencies, see Table II) in the ballscrew, then the input power to the ballscrew can be expressed as

$$P_{BS1} = \max\left(P_{S1}/\eta_{BS12}, P_{S1}\eta_{BS21}\right) \tag{4}$$

where the two terms in the bracket are ballscrew input power when forward- and back-driving respectively.

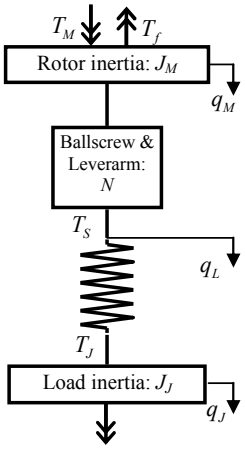

Fig. 3. SEA drivetrain diagram.

Ballscrew screw inertia is too small and therefore ignored; ballscrew nut is rigidly coupled to the rotor, and its inertia is lumped to rotor inertia.

The variable gear ratio N is a nonlinear function of leverarm position q_L (see Fig. 1). The geometrical equations are

$$\begin{aligned} l(q_L) &= \sqrt{r_P^2 + r_D^2 + 2r_P r_D \cos(q_L)} \\ d(q_L) &= r_P r_D \sin q_L / l(q_L) \\ N(q_L) &= d_L(q_L) \cdot 2\pi / p_{BS} = \dot{q}_M / \dot{q}_L \end{aligned} \tag{5}$$

3) Motor

The motor output torque can be calculated using

$$T_M = \begin{cases} \dfrac{T_S}{\eta_{BS12} N} + J_M \ddot{q}_M + T_f + T_{unknown} & P_{BS1} \geq 0 \\ \dfrac{\eta_{BS21} T_S}{N} + J_M \ddot{q}_M + T_f + T_{unknown} & P_{BS1} < 0 \end{cases} \tag{6}$$

where J_M is the lumped moment of inertia of rotor and ballscrew nut; T_f is bearing friction which is a function of motor speed and the actuator axial load; $T_{unknown}$ is other unknown (therefore not modeled) torque terms (cogging torque and windage, etc.).

Then the motor bearing friction power loss, rotor inertial power loss, and motor mechanical output power are

$$\begin{aligned} P_{MI} &= J_M \ddot{q}_M \dot{q}_M \\ P_f &= T_f \dot{q}_M \\ P_{M2} &= T_M \cdot \dot{q}_M = P_{BS1} + P_{MI} + P_f \end{aligned} \tag{7}$$

Knowing the motor torque and speed, we could calculate the motor current, terminal voltage, and motor copper loss

$$\begin{aligned} i_M &= T_M / K_T \\ U_{4q} &= R_M i_M + \dot{q}_M / K_T \\ P_{Cu} &= i_M^2 R_M \end{aligned} \tag{8}$$

The input power to the motor equals

$$P_{M1} = P_{M2} + P_{Cu} \tag{9}$$

4) Motor drive electronics and battery

In the current model, drive electronics and battery dynamics are not modeled. Assuming drive electronics forward and backward efficiency $\eta_{4q12} = \eta_{4q21} = 90\%$ and battery charge/ discharge efficiency $\eta_{B12} = \eta_{B21} = 85\%$, we have

$$\begin{aligned} P_{4q1} &= \max\left(P_{M1}/\eta_{4q12}, P_{M1}\eta_{4q21}\right) \\ P_{B1} &= \max\left(P_{4q1}/\eta_{B12}, P_{4q1}\eta_{B21}\right) \end{aligned} \tag{10}$$

Energy consumption during one gait cycle equals

$$E_{B1} = E_{B1}(r_P, r_D, q_{L0}) = \int_{t=0}^{t=t_{gait}} P_{B1} dt \tag{11}$$

where t_{gait} is duration of one gait cycle. Positive energies indicate that the battery is discharged.

D. Optimization of Joint Drivetrain Design

In the exoskeleton design, for a given task (e.g. mimicking human walking at a speed of 0.8m/s for 8 hours), two steps are taken to minimize the total mass of the drivetrain.

Step-1 optimize the design parameters (geometry) so that the energy consumption is minimized for each possible combination;

Step-2 find the lightest combination of motor, gear system and battery.

*1) **Step-1** Optimization*

For a specific combination of motor and ballscrew, the objective is to minimize the energy consumption by optimizing the geometrical parameters, that is, the proximal and distal leverarm lengths, r_P, r_D, and the initial distal leverarm angular position w.r.t. the proximal leverarm, q_{L0}

$$\min E_{B1}(r_P, r_D, q_{L0}) \tag{12}$$

subjected to the following mechanical and electrical constraints

$$\begin{cases} q_{L\max} - \pi \leq 0 & \text{singularity, } a) \\ (D_J + D_{BS})/2 - d(q_{L\min}) \leq 0 & \text{interference, } b) \\ l_{\min} - l(q_{L\max}) \leq 0 & \text{min actuator length, } c) \\ l(q_{L\min}) - l_{\max} \leq 0 & \text{max actuator length, } d) \\ F_{BS\max} - F_{axial\max} \leq 0 & \text{axial load limit, } e) \\ i_{M\max} - i_{4q\max} \leq 0 & \text{current constraint, } f) \\ U_{4q\max} - \eta_{4q12} U_S \leq 0 & \text{voltage constraint, } g) \end{cases} \tag{13}$$

with $q_{L\min}$ and $q_{L\max}$ the min. and max. leverarm angular position, $l_{\min}$ and $l_{\max}$ the min. and max. actuator length; $i_{M\max}$ and $i_{4q\max}$ are peak motor current and permitted motor current; $F_{BS\max}$ and $F_{axial\max}$ are peak ballscrew axial force and permitted axial force limited by bearings and ballscrew.

Furthermore, the boundary conditions are

$$\begin{cases} r_D \in [r_{D\min}, r_{D\max}] & \text{bounds for } r_D \\ r_P \in [r_{P\min}, r_{P\max}] & \text{bounds for } r_P \\ q_{L0} \in [q_{L0\min}, q_{L0\max}] & \text{bounds for } q_{L0} \end{cases}$$

For each combination of candidate electric motors and ballscrews, an optimal parameter triple r_P, r_D, q_{L0} could be found. Taking the combination of Hacker A60-7SV2 motor and SD12x4 ballscrew as an example, at KFE joint, detailed energy consumption breakdown for all components in the drivetrain is

shown in Fig. 4. An overview for other joints is shown in Table V. Based on the results, we can conclude

- An efficient motor is paramount for this type of application, since copper loss (11.18J per step for KFE, see ΔE_{Cu} in Table V for other DOFs) is one of the major loss sources. Copper loss has to be minimized to improve the overall system efficiency;
- The relatively larger rotor inertia of outrunners does not necessarily cost more energy (see ΔE_{MI} in Fig. 4 and Table V), which can be explained by the almost evenly distributed positive and negative powers about horizontal axis;
- The large power fluctuations (P_{MI}) due to rotor inertia at the second half of the gait cycle do not introduce extra copper loss, because no direct correlation between P_{MI} and P_{Cu} could be seen (see Fig.4, bottom). The rotor inertia is actually assisting the braking of the joint where P_{MI} is negative.

We have to mention that when the full exoskeleton is walking, the motors that are working in generator mode could transfer energy to the motoring motors directly, with only Joule loss in the power cables, which makes the fully-powered exoskeleton slightly more efficient. This concept will be elaborated in our later publications.

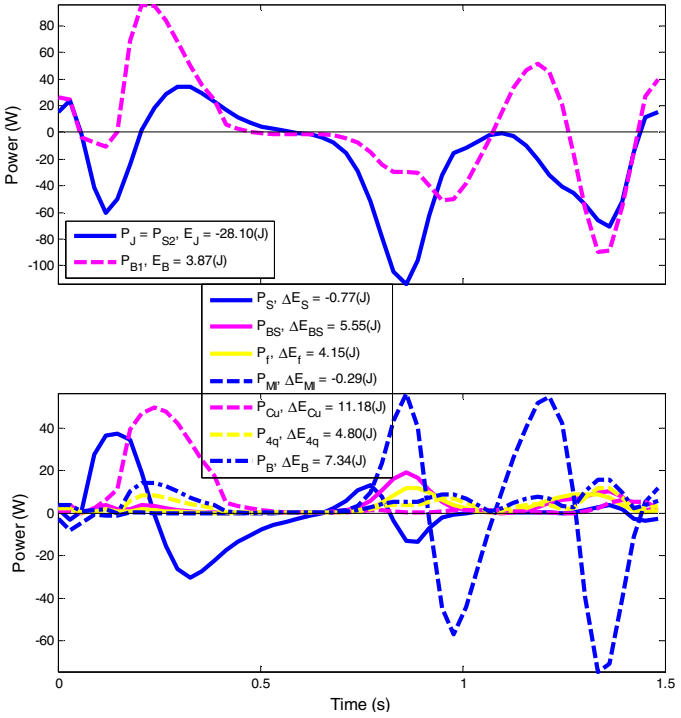

Fig. 4. Step-1 optimization result. Energy consumption breakdown at KFE. **Top:** Power curves are calculated using (2)~(10). Energy is the integral of power over one gait cycle. **Bottom:** Energy consumption at each component by calculating the difference between the input powers and output powers. The knee joint is a very special case where large amount of energy is regenerated (E_J <0) rather than consumed. Throughout the drivetrain, the regenerated energy at the joint is dissipated gradually. Spring and rotor inertia adds 0.77J (ΔE_S) and 0.29J (ΔE_{MI}) to the system respectively. Ballscrew friction, bearing friction, motor winding, drive electronics, and battery costs 5.55J (ΔE_{BS}), 11.18J (ΔE_{Cu}), 4.80J (ΔE_{4q}), and 7.34J (ΔE_B), respectively.

TABLE V. ENERGY CONSUMPTION BREAKDOWN AT FOUR POWERED DOFS

DOFs	HFE	KFE	ADP	HAA
Joint output energy E_J (J)	6.63	-28.10	-3.07	4.80
@Spring ΔE_S (J)	-0.75	-0.77	-1.06	0.43
@Ballscrew ΔE_{BS} (J)	6.38	5.55	1.85	1.42
@Motor bearing ΔE_f (J)	2.79	4.15	1.18	0.64
@Rotor (inertial loss) ΔE_{MI} (J)	-0.24	-0.29	0.08	0.01
@Winding (copper loss) ΔE_{Cu} (J)	11.29	11.18	10.78	11.35
@Drive electronics ΔE_{4q} (J)	5.17	4.80	2.08	2.28
@Battery ΔE_B (J)	8.67	7.34	3.47	3.99
Total input energy E_B (J) [a]	39.94	3.87	15.31	24.92

[a.] equal to the column sum .

2) *Step-2 Optimization*

To compare different combinations, total *mass* was chosen as the common measure. Energy is related to mass after divided by energy density of chosen battery technology.

$$\min f\left(E_B, m_M, m_{BS}\right) = \frac{t_{OP}}{t_{gait}} \cdot \frac{E_B}{\rho_B} + m_M + m_{BS} \qquad (14)$$

with t_{OP} the task duration (8 hours in this paper), ρ_B the battery energy density in J/kg, m_M the motor mass and m_{BS} the ballscrew set mass. Then the first term is the battery mass for certain operation time. The product of task duration t_{OP} and energy consumption per gait E_B affects the final choice of motors and gears. When $t_{OP} \cdot E_B$ is large enough, battery mass dominates the objective function, efficient motors will be the optima; on the contrary when $t_{OP} \cdot E_B$ is small enough, motor mass dominates the objective function, and lighter motors (although less efficient) will be chosen. However there is no uniform strict threshold for $t_{OP} \cdot E_B$ for all the DOFs. In Fig. 5,

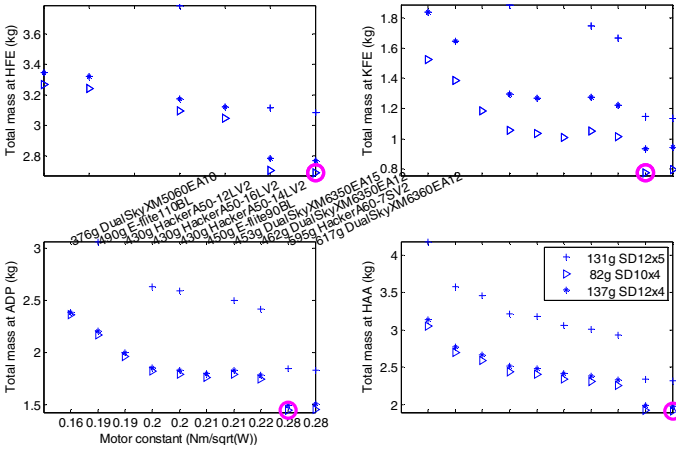

Fig. 5. Step-2 optimization results: total masses of the battery, the ballscrew, and the motor for four powered DOFs. The lightest combinations are encircled by magenta circles. Horizontal axes list out ten motors with their weights (g) and types displayed in the middle; motors are sorted according to motor constants (horizontal axis tick label). Combinations using three different ballscrews are indicated with different markers. The missing markers are combinations that cannot satisfy all constraints. We can conclude that, theoretically for HFE and HAA, DualSky XM6360EA12 and SD10x4 is the best combination (total weight is minimal); Hacker A60-7SV2 and SD10x4 for KFE and ADP. This is because for HFE and HAA the product $t_{OP} \cdot E_B$ (see Table V to compare the E_B values) is much larger than those for other DOFs. Weight difference between the designs using SD12x4 and SD10x4 is mostly less than 50 grams, which is the weight differences of these two ballscrews, because their efficiency difference is marginal (see Table II). The relatively more efficient ballscrew SD12x5 (see Table II) does not result in lightweight design, because its relatively lower gear ratio causes more copper loss and requires heavier battery.

the total masses for different motor and gear combinations are shown. In general motors with higher motor constants lead to lighter designs, which proves the correctness of using motor constant as one of our selection criteria. Abnormities and outliers do exist because not all motors are optimized to their limit in terms of weight and efficiency.

IV. Joint Prototype and Control Implementation

In the current design, the Hacker A60-7SV2 motor and SD12x4 screw were used. According to Fig. 5 SD10x4 is a better ballscrew, but SD10x4 is considered to be sensitive to buckling due to its thin cross-section. The aforementioned components are integrated in a constrained envelope as shown in Fig. 6. The total width of the joint is 90mm and joint diameter is 125mm. The joint without the proximal and distal segments (tubes) weighs 2.9kg. The linear actuator is placed in the center of the joint, and end of the ballscrew is coupled to the leverarm. The disk-shape double spiral spring is to the left of the leverarm and couples the leverarm and the distal segment.

The joint PCB is embedded to the right of the leverarm, which is responsible for communicating with all the encoders and the motor. The drive electronics of the motor is enclosed at the back of the linear actuator, it can provide 24 V and 40A continuous input to the motor, that is, 960W in terms of power. Encoder 1 senses the spring deflection, and encoder 2 measures joint angle, both of which provide 2^{17} counts per revolution. Given the spring stiffness of 820Nm/rad, the effective torque sensing resolution is 0.08 Nm (considering 16 effective bits). The joint PCB has dual EtherCAT E-Bus ports. A PC with EtherCAT master installed can communicate with the joint PCB via EtherCAT coupler EK1100 from Beckhoff. The EtherCAT master is installed under Ubuntu 10.04 with real-time kernel and it interfaces with Matlab/Simulink.

The torque and impedance controller implementations are shown in Fig.7. These controllers update at 2kHz. The motor is treated as a velocity source with its velocity control loop embedded in the joint PCB firmware, updating at 20kHz. The torque loop is closed using the spring deflection measurement using encoder 1, and the impedance loop using the joint encoder measurement.

V. Preliminary Performance Tests

To test the torque control performance, the proximal and distal segments (tubes) of a knee joint are both fixed to a large aluminum plate (Fig.6). To measure the torque control bandwidth at different toque amplitudes, the actuator was commanded to follow a chirp torque setpoint with its frequency changing from 0.1Hz to 50Hz and amplitude from 2Nm to 100Nm. For the 100Nm torque tracking measurement, the time domain signals and the bode plot of the closed-loop transfer function are depicted in Fig.8. The large torque (100Nm peak-to-peak) control bandwidth is over 6Hz. The torque control bandwidth increases as the torque amplitude decreases. The small torque (2Nm peak-to-peak) bandwidth is about 38 Hz. The main characteristics of the joint are summarized in Table VI. All design requirements are met or surpassed.

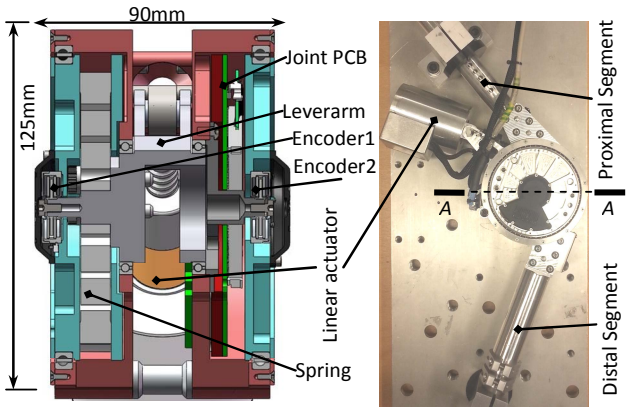

Fig. 6. **Left:** A-A cross-section view of the joint shown on the **Right**. The joint has a sandwich structure, with the linear actuator and the leverarm in the center, to the left is the disk-shape spiral spring, to the right is the embedded joint PCB. **Right:** photo of the exoskeleton joint. In torque control tests, both proximal and distal segments were fixed to the big aluminum plate.

TABLE VI. Specs of the Exoskeleton Joint

Peak torque	100 Nm
Peak power	960 W
Series spring stiffness	820Nm/rad
Small torque bandwidth @ 2Nm	38.2 Hz
Large torque bandwidth @ 100Nm	6.7 Hz
Output torque resolution	0.08 Nm
Closed-loop control update frequency	2000 Hz
Joint mass	2.9 kg

VI. Conclusions

In this paper we present a novel SEA design concept consisting of a linear actuator and a relatively stiff series spring (820Nm/rad) which is a disk-shape double spiral spring made of a single piece of titanium. The linear actuator is very compact thanks to its hollow stator which allows the ballscrew to pass through its core. To achieve a lightweight wearable exoskeleton design, we propose a power-based quasi-static modeling framework for the actuation drivetrain of the joint, which can facilitate the design parameter optimization and

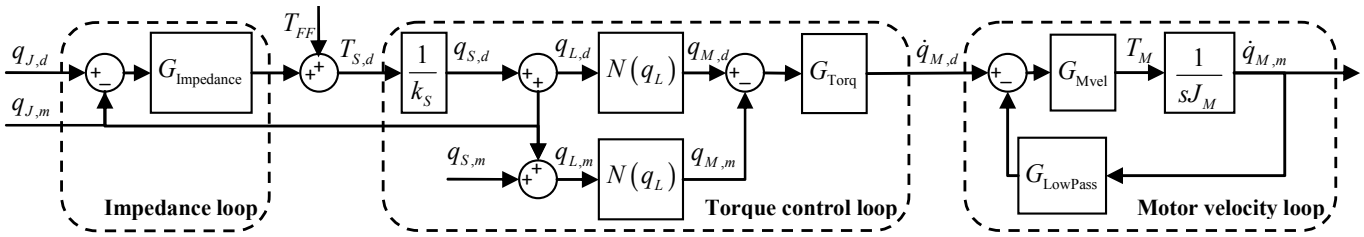

Fig. 7. Controller implementation. Motor is treated as velocity source. Variable gear ratio is compensated in the torque control loop. Joint torque control problem is converted to motor position control problem. $G_{\text{Impedance}}$, G_{Torq} and G_{Mvel} are joint impedance controller, joint torque controller, and motor velocity controller respectively. Quantities suffixed with $_{,m}$ are either directly measured by sensors (encoders) or calculated based on direct measurements; quantities suffixed with $_{,d}$ are the desired signals.

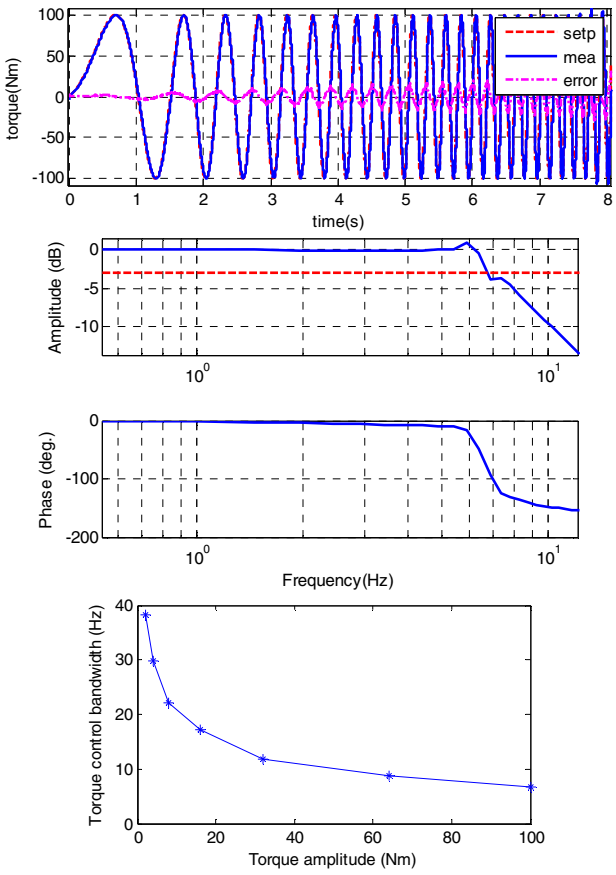

Fig. 8**. Top:** time domain signals for 100Nm chirp torque tracking. The torque setpoint (setp), the measured joint torque (mea), the error are shown in one plot. **Middle:** Bode plot of the closed-loop transfer function for large torque tracking. The joint was commanded to track a chirp signal with amplitude 100Nm and frequency increase slowly from 0.1Hz to 15Hz. The large torque control bandwidth is over 6Hz. **Bottom:** torque control bandwidth at different torque amplitudes. The small torque (2Nm) control bandwidth is over 38Hz. Torque control bandwidth decreases as torque amplitude increases.

component selection process. This framework is readily to be extended, e.g., by replacing ballscrews with other type of gear systems, or replacing the simple model of a component with more advanced model. The power-based quasi-static model of the drivetrain helps to understand a) that in general motors with larger motor constant are more energy efficient and they are heavier, but when long operation time is demanded, these motors can lead to a lightweight design for the actuation and power system; b) that relatively larger moment of inertia does not necessarily introduce extra energy loss for walking gait.

We also present the Mindwalker exoskeleton joint prototype. The joint prototype surpasses our design requirements. The double spiral spring exhibits good linearity (99.99%) and weighs 220g. In combination with the high resolution encoder, it can sense the torque between 0.08Nm and 100Nm. The actuator can output 960W power and can track large torque (100Nm) command up to 6Hz. The joint prototype excluding the segment tubes weighs 2.9kg.

In this paper, we focused on the drivetrain weight minimization. Other aspects of the design need more efforts in the future. For example, the weight of supporting structure which hosts these components also needs to be minimized; better industrial design such as smooth external surfaces and reduced gap sizes would also be critical for safer usage of this device. These are futures steps to be taken for a next prototype.

VII. Acknowledgement

The research is supported by the EU FP7 grant no.:247959. I would like to thank Arthur Ketels (Speciaal Machinefabriek Ketels v.o.f., the Netherlands) for providing us the custom-made high power electronics and EtherCAT technology support.

References

[1] M. Wyndaele, J..J. Wyndaele, “Incidence, prevalence and epidemiology of spinal cord injury: what learns a worldwide literature survey?” Spinal Cord 44:523–508, 3 January 2006.

[2] ARGO Medical Technology Ltd., http://www.argomedtec.com/, 2013

[3] Ekso Bionics, http://www.eksobionics.com/ekso, 2013

[4] REX Bionics, http://www.rexbionics.com/, 2013

[5] D.E. Whiteney, “Force feedback control of manipulator fine motions,” J. Dyan. Syst. Measurement Control, 99:91-97, 1977

[6] https://mindwalker-project.eu/, 2013

[7] J. Kessels, “Energy Management for Automotive Power Nets,” PhD thesis, Department of Mechanical Engineering, Technische Universiteit Eindhoven, The Netherlands, 2007.

[8] S. Wang, W. v. Dijk, H.v.d. Kooij, “Spring uses in exoskeleton actuation design,” IEEE Int. Conf. on Rehab. Robotics, Zurich, Switzerland, 2011

[9] P. D. Neuhaus, J. H. Noorden, T.J. Craig, T. Torres, J. Kirschbaum, J. E. Pratt, “Design and evaluation of Mina: A robotic orthosis for paraplegics,” IEEE Int. Conf. on Rehabilitation Robotics, Zurich, Switzerland, 2011.

[10] K.W., Hollander, R., Ilg, T.G., Sugar, D., Herring, “An efficient robotic tendon for gait assistance,” J. of Biomechanical Engineering, 128:788-791 , 2006.

[11] D. Hanselman, “Brushless Permanent Magnet Motor Design,” second edition, Magna Physics Pub., 2006

[12] F. Magnussen and C. Sadarangani, “Winding Factors and Joule Losses of Permanent Magnet Machines with Concentrated Windings,” IEEE Int. Electric Machines and Drives Conference (IEMDC'03), p. 333-338, Madison, USA, 2003.

[13] A.H.A. Stienen, E.E.G. Hekman, H. ter Braak, A. M. M. Aalsma, F. C. T. van der Helm, H. van der Kooij, “Design of a Rotational Hydroelastic Actuator for a Powered Exoskeleton for Upper Limb Rehabilitation”, IEEE Transactions on Biomedical Engineering, 57:728-725, 2010.

[14] C. Lagoda, A. C. Schouten, A. H. A. Stienen, E. E. G. Hekman, H. van der Kooij, “Design of an electric series elastic actuated joint for robotic gait rehabilitation training,” IEEE RAS and EMBS Int. Conf. on Biomedical Robotics and Biomechatronics (BioRob), Tokyo, Japan, p. 26-29, 2010.